Measurements of Inertial Limit Alfvén Wave Dispersion for Finite Perpendicular Wave Number

C. A. Kletzing,[1,*] D. J. Thuecks,[1] F. Skiff,[1] S. R. Bounds,[1] and S. Vincena[2]

[1]*Department of Physics and Astronomy, University of Iowa 203 Van Allen Hall, Iowa City, Iowa, 52245, USA*

[2]*Department of Physics and Astronomy, University of California Los Angeles 1000 Veteran Avenue, Suite 15-70, Los Angeles, California, 90095-1696, USA*

(Received 24 April 2009; published 2 March 2010)

Measurements of the dispersion relation for shear Alfvén waves as a function of perpendicular wave number are reported for the inertial regime for which $V_A > V_{Te}$. The parallel phase velocity and damping are determined as $k_\perp$ varies and the measurements are compared to theoretical predictions. The comparison shows that the best agreement between theory and experiment is achieved for a fully complex plasma dispersion relation which includes the effects of electron collisions.

DOI: 10.1103/PhysRevLett.104.095001 PACS numbers: 52.35.Hr, 52.72.+v

The Alfvén wave, predicted by Alfvén in 1942, is one of the most fundamental plasma waves in space and in the laboratory [1]. Alfvén waves have been found in the magnetopause associated with magnetic reconnection and in the solar wind as the primary wave mode dominating the turbulent spectrum found there. In space, these waves are thought to be a primary mechanism mediating magnetosphere-ionosphere coupling, and several models have shown that these waves can accelerate electrons in the Earth's auroral zone, producing electron signatures similar to those observed on rockets and satellites [2–5]. Space-based auroral zone observations have also verified the correct E/B ratio for these waves [6,7].

Measurements of Alfvén waves in the laboratory were first made in the 1950s [8–10]. Most recently, laboratory experiments have focused on their characteristics for narrow perpendicular scales [11–15]. Although the dispersion relation for these waves has been derived by several authors, direct experimental measurements to verify the physics of shear ($\delta B \perp B_0$) Alfvén waves in the limits where the perpendicular scale of the waves becomes comparable to either the electron skin depth or the ion acoustic gyroradius (the gyroradius of ions with the electron temperature) have been few. The work we report here focuses on the so-called "inertial" limit in which the electrons are cold relative to the wave speed ($V_A > V_{Te}$). In this limit, the electron skin depth is the relevant length scale. These measurements allow us to test theoretical predictions of the dispersion of these waves by direct comparison with data.

Experimental setup and analysis.—The experiments we describe were conducted in the Large Plasma Device (LAPD) at University of California, Los Angeles, which produced a plasma column of 16.5 m length and ~40 cm diameter. The experiments took place in a fully ionized, discharge helium plasma 0.91 ms after the discharge ended with density determined by a swept Langmuir probe to be 7.7×10^{11} cm^{-3}, calibrated with a microwave interferometer. The electron temperature was measured with a swept Langmuir probe and found to be 1.9 eV in the region where the waves were launched. No temperature measurements were made of the ions, but they are assumed to have a temperature of ~1.25 eV based on interferometric measurements made under similar plasma conditions. The background magnetic field was set at 2300 G, which yields ratios of electron thermal speed to Alfvén speed of $V_{Te}/V_A = 0.20$, corresponding to the inertial limit. For these plasma parameters, the skin depth, $\delta_e = c/\omega_{pe}$, was 0.61 cm and the ion acoustic gyroradius, $\rho_s = (T_e/m_i)^{1/2}/\omega_{ci}$, was 0.13 cm. The waves were launched using a windowed tone burst of ten periods at two frequencies of 250 and 380 kHz which give ratios relative to the ion cyclotron frequency ω_{ci} of $\omega/\omega_{ci} = 0.29$ and $\omega/\omega_{ci} = 0.43$, respectively.

To produce the narrow perpendicular wavelengths of interest, we have developed an antenna consisting of a set of 48 vertical grids which can be driven with a temporally identical signal on each grid, but with varying amplitudes from 1 to −1 (inverted phase) for each element. A schematic of the antenna is shown on the left-hand side of Fig. 1. The view shown is along the background, axial magnetic field ($\hat{z}$ direction). The grids are located on 0.64 cm centers with dimensions of 2.5 cm × 30.5 cm and are made of coarse copper mesh to make good contact with the plasma. Viewed edge-on in Fig. 1 (left), they appear as vertical lines. By driving each grid with varying amplitudes that are locked together in time, we can synthesize an arbitrary spatial waveform across the grid array in the $\hat{x}$ direction with effectively no variation in the $\hat{y}$ direction.

Each grid element is driven by an individual amplifier providing a current of up to 10 A. The output signal can be inverted relative to the input signal giving 180° phase shift. Each amplifier has a bias circuit which can be set, if needed, to positively bias the grid to allow larger amplitudes without being limited by the ion saturation current. The final output of the amplifier combines the bias signal and the amplified input signal. An example of a sinusoidal pattern is shown in the right-hand side of Fig. 1. This shows a temporal snapshot of a full data plane of the B_y component of a propagating Alfvén wave. The data appear

 © 2010 The American Physical Society

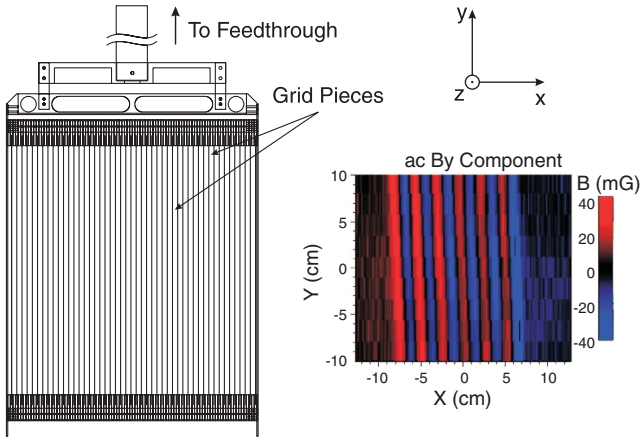

FIG. 1 (color). The arbitrary spatial waveform antenna (left) consists of 48 grids that can be driven separately to produce arbitrary waveforms along the x axis (across the grids). An example of a plane of B_y magnetic field measurements showing a snapshot in time of a propagating Alfvén wave with narrow perpendicular structure is shown at right. The antenna was slightly rotated from purely vertical, producing the slanted appearance.

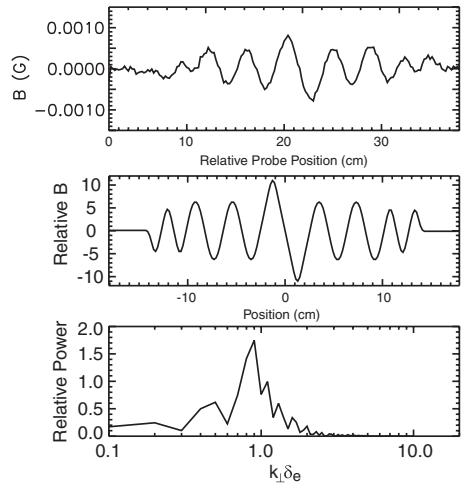

FIG. 2. Example of the measured (top panel) and desired (middle panel) waveform patterns generated using the arbitrary spatial waveform antenna. The pattern is a midplane cut of the vertical component of the magnetic field (B_y) of a propagating Alfvén wave at a single instant in time. The bottom panel shows the theoretical $k_\perp$ spectrum based on the pattern in the middle panel.

slightly slanted due to a small rotation of the antenna relative to the vertical.

Initially, we used simple patterns approximating a single wavelength sinusoid. However, it became apparent that combining several $k_\perp$ values into a single pattern provided coverage of a larger piece of the $k_\perp$ spectrum more efficiently. Figure 2 shows an example of such a pattern measured in the LAPD plasma. The top panel is a line of data scanned across the center of the antenna in the $\hat{x}$ direction and shows the vertical ($\hat{y}$) component of the magnetic field of a propagating Alfvén wave at a single instant in time, illustrating the structure in the perpendicular component of the wave. The middle panel of Fig. 2 shows the predicted pattern based on the settings of the antenna drive currents. The agreement between the measured pattern and the model pattern is good. The bottom panel shows the $k_\perp$ spectrum calculated from the theoretical pattern, demonstrating that a range of values is generated at one time. This illustrates the flexibility of this scheme; rather than designing new antennas for each kind of spatial waveform, we synthesize the desired pattern by setting the amplitudes of the signals driving each grid.

To compare with theory, we determine the parallel phase velocity and damping of inertial Alfvén waves as a function of $k_\perp$. The experimental procedure is to set up a given antenna pattern and then drive the grids with a windowed, ten period tone burst at a fixed frequency. The windowing provides a ramp-up and ramp-down of the amplitude over the first and last period of the tone burst to reduce transients as the wave is launched. Because the grid pieces are extended in the vertical ($\hat{y}$) direction, the measurements used for this experiment were taken from the midplane of the antenna pattern, halfway between the top and bottom. This allows us to analyze the data as if the wave pattern were infinite in the vertical direction, reducing the problem to a two dimensional one in $k_\parallel$ ($\hat{z}$, along the machine axis) and $k_\perp$ ($\hat{x}$, horizontally across the pattern). For each tone burst frequency, four different spatial waveform patterns were used to give good coverage of $k_\perp$.

The wave magnetic field was measured with three-axis search coil probes ("b-dot" probes) consisting of 40 loops in each orthogonal direction and loop diameter of 1.2 mm. To improve signal quality, the probes have amplifiers located inside the plasma chamber. Samples are taken in horizontal lines across the plasma column with 2 mm spacing. In time, each location is sampled at 12.5 Msamples/s resolution. The excellent repeatability of the LAPD allows us to average 30 shots at each measurement location to reduce noise and better resolve the wave signal.

To determine parallel phase velocity and damping, a line of data is Fourier-transformed in space at each time step to yield the perpendicular wave number spectrum as a function of time. Implicit in this technique is the assumption that we may ignore variation in the vertical direction as discussed above. As Fig. 1 shows, this is a reasonable assumption due to the lack of variation along the vertical direction near the center of the wave pattern. This procedure is then repeated for a second location farther away from the antenna, and the two Fourier-transformed data sets are compared to determine the wave dispersion properties.

The measurements are analyzed with a chi-square fitting procedure that assumes that the difference between the second waveform and the first arises from a propagation time delay and an amplitude decrease due to damping. We solve for the time delay and amplitude factor by minimizing the value of chi square of the two data sets. The time delay is also checked by performing a linear cross corre-

lation between the two signals of the type used for statistically relating arrays of numbers. For all data shown here, the R value of the cross correlation was 0.90 or greater, confirming the assumption that the signal at the two measurement locations is the same wave which has propagated along the magnetic field. Both procedures yield the same time delay. The advantage of the chi-square procedure is that it also yields amplitude change as well as the errors associated with the fitted time delay and amplitude factor. This is the same procedure that we have used successfully in earlier experiments, and a more complete description may be found in [14].

The time delay is combined with the measured distance of 1.92 m between the two sets of measurements to determine the phase velocity. The chi-square–correlation technique is optimized to produce the greatest correlation for alignment of the peaks of the two waveforms rather than the envelope of the waveform. This ensures that the velocity which is found corresponds to the parallel phase velocity of the wave $v_{\mathrm{ph},\parallel} = \omega/\mathrm{Re}(k_\parallel)$ and not the group velocity. By repeating this procedure at each wave number with significant power above the background noise level, a set of measurements of the parallel phase velocity as a function of perpendicular wave number is generated. The fitting procedure also determines the decrease in amplitude which corresponds to the spatial damping rate. For $k_\perp \delta_e \leq 0.5$, the damping is weak enough that some power is reflected from the end of the LAPD and interferes with the latter portion of the forward propagating wave packet. For these wave numbers, only the first 2–3 periods of the tone burst are used for the time delay and damping determinations so as to ensure that we compare only the forward propagating parts of the wave. For all data, the very slight rotation of the antenna evident in Fig. 1 is negligible and does not affect the results.

The results of this procedure are shown for all four sets of antenna patterns for a tone burst of 380 kHz in Fig. 3. The upper panel shows measurements of the phase velocity and the lower panel shows those of the damping. The perpendicular wave number is normalized to the plasma skin depth δ_e and the phase velocity is normalized to the background Alfvén speed $V_A = B/\sqrt{4\pi n m_i}$. For comparison, the warm-plasma theoretical curve with collisions is shown as a solid black line. The error bars on each point include timing, length, and fitting uncertainties. Uncertainty in the background magnetic field magnitude as well as fluctuations of the temperature and density are shown by two black dash-dotted bounding curves to show clearly how these fluctuations affect the result. The model curves use the temperature determined by the Langmuir probe, but use a density of 6.5×10^{11} cm^{-3} instead of the 7.7×10^{11} cm^{-3} determined by the probe. The excellent fit of the data to this lower density suggests a systematic error in the Langmuir probe density calibration which was the same for all data presented here. Consequently, we use this lower value for comparisons to theory.

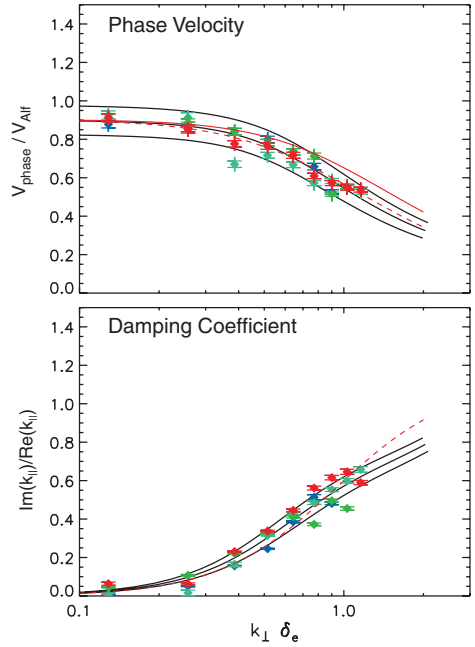

FIG. 3 (color). A comparison of the dispersion relation with the measurements as a function of $k_\perp$. The data are from four antenna patterns (different colors) for identical plasma conditions with a tone burst of 380 kHz. The theoretical dispersion relation with collisions is plotted as a solid black line. Uncertainties in plasma parameters are shown as bounding dash-dotted curves. The solid red curve shows the comparison with the dispersion relation given by (1) with $\nu/\omega = 0$ and the red-dashed curve the case for $\nu/\omega = 2.7$. The lower panel shows wave damping.

A second set of measurements shown in Fig. 4 was made under the same set of plasma conditions, but the tone burst frequency was lowered to 250 kHz. This was done both to validate that the inertial Alfvén wave propagates at a variety of frequencies as well as to investigate the small change in the dispersion relation as a function of frequency relative to the ion cyclotron frequency ω_{ci}. As can be seen, for both cases, the agreement between theory and measurement is good.

Discussion and conclusions.—Because the electrons have finite temperature and the wave frequency is of the order of the ion cyclotron frequency, the simplification of the dispersion relation that results for the inertial case that assumes $T_e = 0$ is not the most accurate for use with these results. For the best comparison with data, we numerically solve the full warm-plasma dispersion relation for finite frequency with respect to the ion gyrofrequency, keeping all terms in the dielectric tensor. Additionally, a nonconserving Krook collision operator is used to include the effect of electron collisions which are not negligible. A complete discussion of this and other operators is found in [16]. In this solution, ω and $k_\perp$ are kept real and $k_\parallel$ is complex. This correctly handles the damping that we measure, which is determined as a function of position as the wave propagates [17]. This is the solution plotted in black in Figs. 3 and 4.

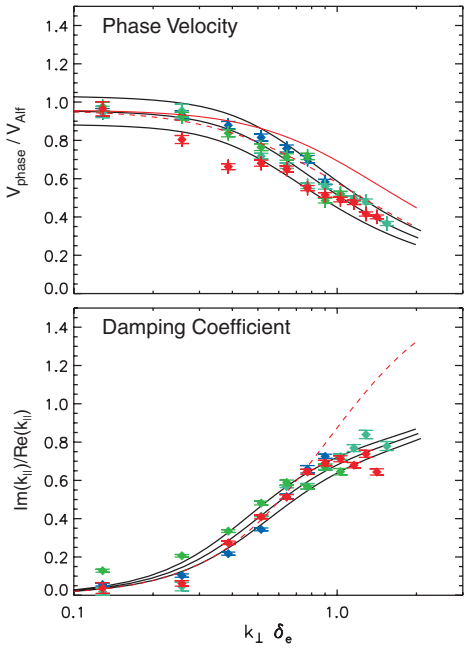

FIG. 4 (color). A comparison of the dispersion relation and measurement for the case in which the tone burst frequency was 250 kHz. The format is the same as Fig. 3.

Although warm-plasma theory with collisions gives the most precise dispersion relation for comparison with the measurements, it does not provide the most intuitive form for understanding the physics. For this we turn to a simplified dispersion relation with cold electrons ($V_A \gg V_{Te}$), but retain the finite frequency effects. The collisionless dispersion relation has been derived by several authors, e.g., [6], but is modified here to include electron collisions:

$$\frac{\omega}{k_{\parallel}} = V_A \sqrt{\frac{(1 - \omega^2/\omega_{ci}^2)}{1 + k_{\perp}^2 \delta_e^2 (1 + i\nu/\omega)}}, \qquad (1)$$

where ρ_s is the ion acoustic gyroradius and δ_e is the plasma skin depth. Collisions are added by taking $m \rightarrow m(1 + i\nu/\omega)$ which properly introduces collisions only in the electron momentum equation. This dispersion relation is shown as a red dashed curve in Fig. 3 for $\nu/\omega = 2.7$ and Fig. 4 for $\nu/\omega = 4.1$. The solid red curve in both figures is the $\nu/\omega = 0$ case of (1). These curves do not fit the data quite as well as the full theory, but still do a good job of matching the data. The form of (1) shows how the parallel phase velocity depends on $k_{\perp}$ and that measurement of the parallel phase velocity directly verifies the dispersion relation (1). The electron kinetic effects are clearly seen in the upper panels of Figs. 3 and 4—the phase speed decreases as the perpendicular length scale decreases to the scale of the plasma skin depth as expected in the inertial limit.

The effects of finite frequency are also apparent in the form given by (1). For both cases presented here, there is a small decrease in the phase velocity due to this effect. The change is greatest for the 380 kHz case, and this is reflected in the y intercept at low values of $k_{\perp}$, which shows that the phase speed is reduced relative to that of the MHD Alfvén speed.

The lower panels of Figs. 3 and 4 show the experimentally determined damping. It is important to note that Landau damping alone is not sufficient. Indeed, it is essentially zero for all the data in the two figures. To illustrate this, we compare the red dashed curves in Figs. 3 and 4, which show the collisional damping from (1), with the black curves from the full warm-plasma theory. The excellent agreement, except at higher $k_{\perp}$, shows both that the damping is completely dominated by collisions and also that the simple form of (1) does a very good job of describing the data. The damping also affects the real part of the dispersion relation by lowering the phase velocity for wave numbers where the damping is significant. The damping is weaker for the 380 kHz case (Fig. 3), and the effect on the phase velocity is not as great resulting in better agreement between the collisional and the collisionless theory. The inclusion of electron collisions clearly produces the best match to the measurements.

We believe these to be the first detailed measurements of the phase velocity and damping as a function of $k_{\perp}$ for Alfvén waves in the inertial limit. The agreement between both the collisional warm-plasma dispersion relation and a simpler collisional fluid version with experiment is very good and provides an important verification of fundamental plasma theory.

This work was performed at the Basic Plasma Science Facility at UCLA under NSF Grant No. ATM 03-17310 and DOE Grant No. DE-FG02-06ER54890. We thank A. Bhattacharjee and W. Gekelman for helpful discussions.

*craig-kletzing@uiowa.edu

[1] H. Alfven, Nature (London) **150**, 405 (1942).
[2] C. K. Goertz and R. W. Boswell, J. Geophys. Res. **84**, 7239 (1979).
[3] R. L. Lysak, J. Geophys. Res. **90**, 4178 (1985).
[4] C. A. Kletzing, J. Geophys. Res. **99**, 11 095 (1994).
[5] C. A. Kletzing and S. Hu, Geophys. Res. Lett. **28**, 693 (2001).
[6] K. Stasiewicz *et al.*, Space Sci. Rev. **92**, 423 (2000).
[7] C. C. Chaston *et al.*, J. Geophys. Res. **111**, A03206 (2006).
[8] W. H. Bostick and M. A. Levine, Phys. Rev. **87**, 671 (1952).
[9] T. K. Allen *et al.*, Phys. Rev. Lett. **2**, 383 (1959).
[10] D. F. Jephcott, Nature (London) **183**, 1652 (1959).
[11] W. Gekelman *et al.*, Phys. Plasmas **1**, 3775 (1994).
[12] W. Gekelman *et al.*, J. Geophys. Res. **102**, 7225 (1997).
[13] D. Leneman, W. Gekelman, and J. Maggs, Phys. Rev. Lett. **82**, 2673 (1999).
[14] C. A. Kletzing *et al.*, Phys. Rev. Lett. **90**, 035004 (2003).
[15] S. Vincena, W. Gekelman, and J. Maggs, Phys. Rev. Lett. **93**, 105003 (2004).
[16] D. J. Thuecks *et al.*, Phys. Plasmas **16**, 052110 (2009).
[17] S. Vincena, W. Gekelman, and J. Maggs, Phys. Plasmas **8**, 3884 (2001).